This study adopted three well-established methods to generate an angular-normalized, cloud-filled, and 0.01°-enhanced LST dataset covering the spatial extent of the FY-4A disk. The methodology is sound, and the validation is comprehensive, which includes both in situ and cross-validation approaches. I have the following suggestions to improve the readability of the manuscript:

Response: Thank you very much for your affirmation on our study and all your professional suggestions to improve the manuscript. We have corrected one-by-one as introduced below (Red represents our response, and blue represents modifications in the manuscript).

1. **Line 283: Please check the formulation of the DTC model equation. It should be a cosine function.**

Response: Thank you for your detailed suggestion. We're sorry for the mistake in DTC equation. We have revised the manuscript accordingly.

In Eq. 6:

$$f_{iso}(t) = T_0 + T_a \times \cos\left[\frac{\pi}{\omega} \cdot (t - t_m)\right]$$

2. **Line 297: A 17-day filter was used to obtain the kernel-driven model parameters, which are related to surface structure. What are the spatial patterns of these parameters?**

Response: Thank you for your comment about the spatial distribution of KDM parameters. Here, we present the KDM parameters over FY-4A disk. Yearly aggregation in 2020 was performed to avoid gaps in frequent cloud cover area. As shown in Fig. R1 (a), the gap fraction kernel coefficient (α) is usually negative, especially in bare soil regions, which indicates the nadir LST is usually higher than off-nadir directions. This trend is similar to recent studies (Ermida et al., 2024). In boreal forest region, α is usually positive, partly attribute to the wet yet cold soil that is usually under the shadow of high forest. For hotspot kernel coefficient, it's very high in mountainous region as shown in Fig. R1 (b). This may be caused by the block of mountains, which amplified the hotspot effect. The hotspot width is usually small in tropical region with dense vegetation (Fig. R1 (c)). This is consistent with the understanding that hotspot influence region is narrower over continuous vegetation, and is always larger in sparsely vegetated area. Overall, the parameters estimated by TEKDM have fine spatial explanation as expected. Considering ESSD pay more attention to the dataset instead of details in TRD correction, we do not add the analysis in revised manuscript. Thank you again for your detailed suggestion.

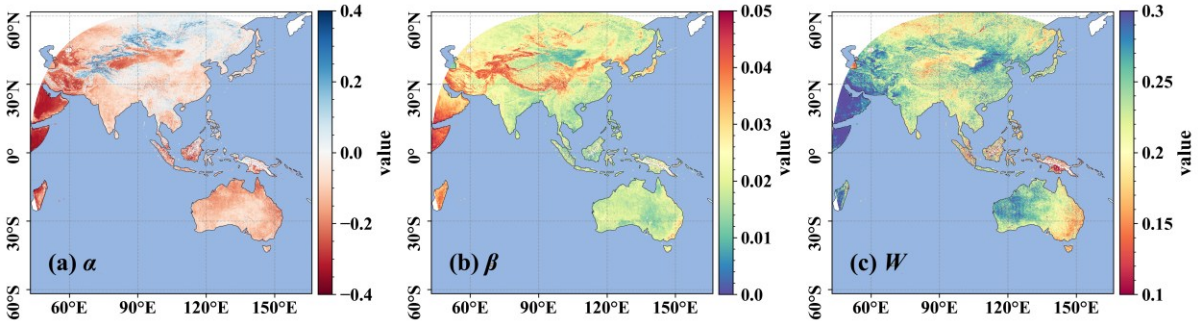

Fig. R1 The spatial distribution of KDM parameters, including (a) gap fraction kernel coefficient α, (b) hotspot kernel coefficient β, and (c) hotspot width W.

Reference:

Ermida, S.L., Hulley, G., Trigo, I.F., 2024. Introducing emissivity directionality to the temperature-emissivity separation algorithm. Remote Sensing of Environment 311, 114280. https://doi.org/10.1016/j.rse.2024.114280

3. Line 306: A third-order polynomial fit was applied to accelerate the calculation of the hemispherical LST. More details about the fitting procedure should be provided—for example, the scatter plot between the accurate T_hemi and the fitted T_hemi.

Response: Thank you for your comment about the hemispherical integration. As shown in the numerator in Eq. 12, the integration for deriving T_{hemi} is only determined by α, β, W, and SZA. Here, we construct a look-up table by traversing α from -0.35 to 0.35 with a step of 0.01, β from 0 to 0.05 with a step of 0.001, W from 0.05 to 0.5 with a step of 0.01, and SZA from 0° to 90° with a step of 1°. Finally, 1,479,880 integration values were derived through accurate but computationally intensive numerical integration. Then, a third-order polynomial fitting was applied with the input of α, β, W, SZA, and K_{Chen} value at nadir, and the output of integration value (i.e., Φ value in Eq. A1).

$$T_{hemi}(t,\theta_s)=\left(\frac{1}{\pi}\cdot\int_0^{2\pi}\int_0^{\pi/2}T_{dir}^4(t,\theta_s,\theta_v,\Delta\varphi)\cdot\cos\theta_v\cdot\sin\theta_v d\theta_v d\varphi_v\right)^{\frac{1}{4}}$$
$$=\frac{T_{dir}\left(t,\theta_s,\theta_v^{FY},\Delta\varphi_v^{FY}\right)\cdot\left(\int_0^{2\pi}\int_0^{\pi/2}\left(1+\alpha\cdot K_{LSF}(\theta_v)+\beta\cdot\cos\theta_s\cdot K_{Chen}(\theta_s,\theta_v,\Delta\varphi,W)\right)^4\cdot\cos\theta_v\cdot\sin\theta_v d\theta_v d\varphi_v\right)^{\frac{1}{4}}}{\pi\cdot\left(1+\alpha\cdot K_{LSF}\left(\theta_v^{FY}\right)+\beta\cdot\cos\theta_s^{FY}\cdot K_{Chen}\left(\theta_s,\theta_v^{FY},\Delta\varphi_v^{FY},W\right)\right)} \quad (12)$$

$$\Phi(\alpha,\beta,W,\theta_s)=\frac{1}{\pi}\left(\int_0^{2\pi}\int_0^{\pi/2}\left(1+\alpha\cdot K_{LSF}(\theta_v)+\beta\cdot\cos\theta_s\cdot K_{Chen}(\theta_s,\theta_v,\Delta\varphi,W)\right)^4\cdot\cos\theta_v\cdot\sin\theta_v d\theta_v d\varphi_v\right)^{\frac{1}{4}} \quad (A1)$$

where Φ is the integration value to be estimated. The fitting performance is shown in Fig. R2 (a), and almost all the data points were aligned well with 1:1 line, with an RMSE of 0.000158. Fig. R2 (b) shows how error in polynomial fitting propagated to final hemispherical LST. We set the isotropic kernel coefficient of 300 K, and randomly sample 10,000 α, β, W, and SZA values. Then, the T_{hemi} estimated via polynomial fitting was evaluated taking accurate numerical integration-derived T_{hemi} as reference value. Results showed two hemispherical LST is consistent, with an RMSE within 0.1 K, which is much smaller than the uncertainty of TRD correction. In revised manuscript, we added this analysis in Appendix A. Thank you again for your detailed suggestion.

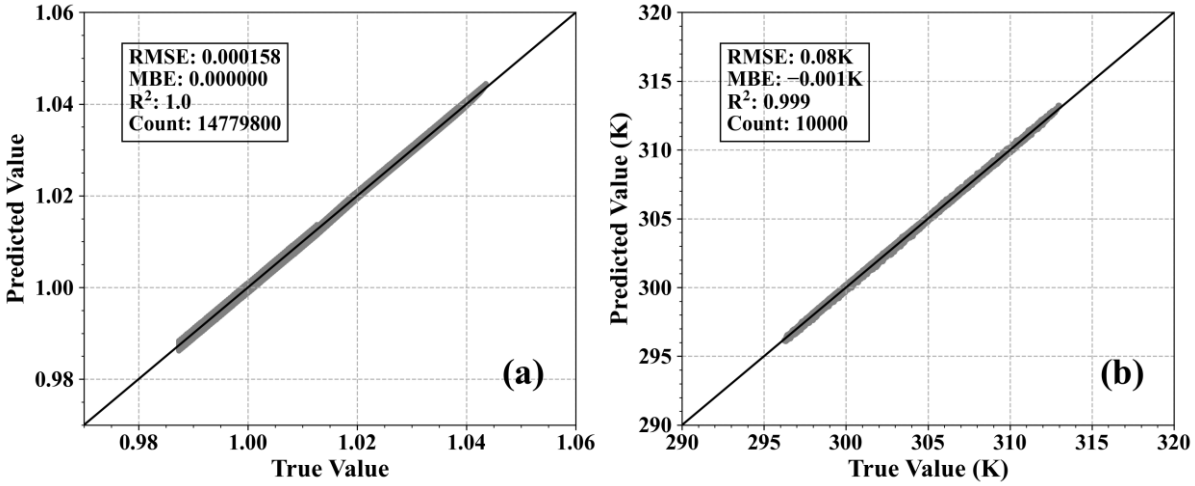

Fig. R2 The performance of polynomial fitting for (a) Φ and (b) T_{hemi}.

In Subsection 3.1:

More details about the integration procedure are provided in Appendix A. As shown in Fig. A1, this polynomial approximation substantially reduces computational cost while introducing an uncertainty of less than 0.1 K.

In appendix A:

Accurate numerical integration for deriving T_{hemi} is computationally expensive. To improve efficiency, a polynomial fitting approach was adopted to approximate the exact integration. As shown in the numerator of Eq. 12, the integration involved in estimating T_{hemi} depends only on α, β, W, and SZA. Accordingly, a look-up table was constructed by traversing α from -0.35 to 0.35 with a step of 0.01, β from 0 to 0.05 with a step of 0.001, W from 0.05 to 0.5 with a step of 0.01, and SZA from 0° to 90° with a step of 1°. In total, 1,479,880 integration values were obtained using accurate but computationally intensive numerical integration. Subsequently, a third-order polynomial was fitted, taking α, β, W, SZA, and K_{Chen} value at nadir as inputs, and the corresponding integration value as the output. Eq. A1 shows the integration target for fitting, while Eq. A2 shows the final computation of T_{hemi}.

$$\Phi(\alpha,\beta,W,\theta_s)=\frac{1}{\pi}\cdot\left(\int_0^{2\pi}\int_0^{\pi/2}\left(1+\alpha\cdot K_{LSF}(\theta_v)+\beta\cdot\cos\theta_s\cdot K_{Chen}(\theta_s,\theta_v,\Delta\varphi,W)\right)^4\cdot\cos\theta_v\cdot\sin\theta_v d\theta_v d\varphi_v\right)^{\frac{1}{4}} \quad \text{(A1)}$$

$$T_{hemi}=f_{iso}\cdot\Phi(\alpha,\beta,W,\theta_s) \quad \text{(A2)}$$

where Φ is the integration value to be estimated. The fitting performance is shown in Fig. A1(a), where nearly all data points closely follow the 1:1 line, yielding an RMSE of 0.000158. Fig. A1(b) shows how errors from polynomial fitting propagate into the final hemispherical LST. Specifically, the isotropic kernel coefficient (f_{iso}) was set to 300 K, and 10,000 sample of α, β, W, and SZA were randomly generated. The T_{hemi} estimated using the polynomial approximation was then evaluated against the reference T_{hemi} derived from accurate numerical integration. The results indicate strong consistency between the two estimates, with an RMSE within 0.1 K, which is substantially smaller than the uncertainty associated with TRD correction.

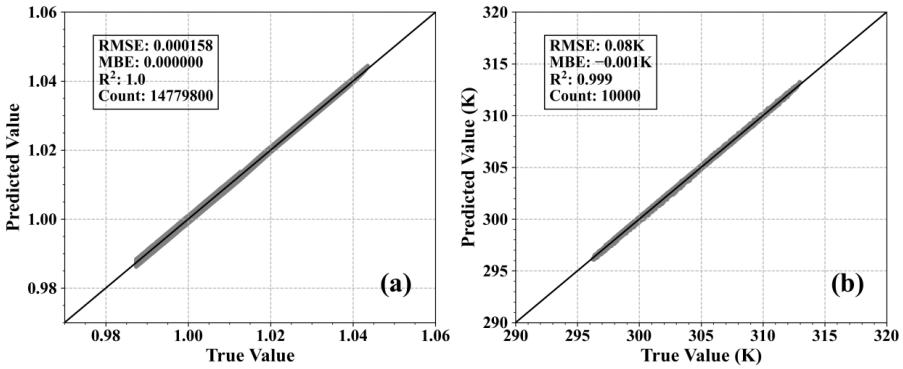

Figure A1: Performance of the polynomial fitting for (a) Φ and (b) T_{hemi}.

4. Line 480: Is there a specific hemispherical equivalent angle for which T_dir equals T_hemi across the FY-4A disk? I wonder if this is consistent with the findings of current studies (i.e., within the 44°–55° range).

Response: Thank you for your suggestion about the hemispherical equivalent angle (HEA). As you suggested, we analyzed the HEA over entire FY-4A disk at the Beijing time of 12:00. Results in Fig. R3 shows the HEA generally varies from 46° to 58°, whit a yearly average of 53.4°. This result is consistent with reported HEA range in Zhang et al. (2025) and Hu et al. (2023), which is in the range of 44°–55° as you mentioned. The above analysis is not included in revised manuscript as it's hard to get a fixed HEA value due to its strong annual variation and deriving a fixed HEA is beyond the scope of this study. Thank you again for your insightful suggestion.

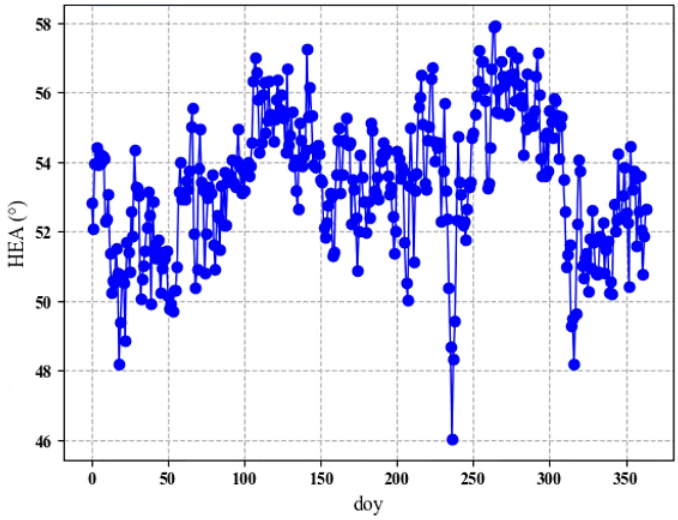

Fig. R3 The annual variation of hemispherical equivalent angle in 2020.

Reference:

Hu, T., Roujean, J.-L., Cao, B., Mallick, K., Boulet, G., Li, H., Xu, Z., Du, Y., Liu, Q., 2023. Correction for LST directionality impact on the estimation of surface upwelling longwave radiation over vegetated surfaces at the satellite scale. Remote Sensing of Environment 295, 113649. https://doi.org/10.1016/j.rse.2023.113649

Zhang, X., Cao, B., Na, Q., Zheng, L., Yang, Z., Qin, B., Bian, Z., Du, Y., Li, H., Xiao, Q., Liu, Q., 2025. Determination of the Hemispherical Equivalent Angle for Surface Upward Longwave Radiation. IEEE Geosci. Remote Sensing Lett. 1–1. https://doi.org/10.1109/LGRS.2025.3558980

5. Some typographical errors should be corrected: -Line 233: "…which had been used in the studies of (Che et al., 2019; Li et al., 2025; Ma et al., 2024b)" should be revised to "…which had been used in previous studies (Che et al., 2019; Li et al., 2025; Ma et al., 2024b)." -Line 577: "We employed the logarithmic value of log(1 + scorenorm) to..." should be revised to "We employed the logarithmic value of (1 + scorenorm)."

Response: Thank you for your detailed review of our manuscript. We have modified the typographical errors as you suggested.

In line 250:

As shown in Fig. 2, 5 sites from the Heihe Watershed Allied Telemetry Experimental Research (HiWATER)

experiment within the Heihe River Basin (HRB) and 3 sites from the Terrestrial Ecosystem Research Network (TERN) OzFlux network in 2020 were selected, **which had been used in LST evaluation studies (Beringer et al., 2016; Che et al., 2019; Li et al., 2025, 2020).** More detailed information on the spatial representativeness of the in situ sites is provided in Subsection 5.3.

In line 595:

We employed **the logarithmic value of (1 + $score_{norm}$)** to quantify the importance of each model (where $score_{norm}$ is the max-min normalized feature scores).